Journal of Geosciences, 66 (2021), 227–242 DOI: 10.3190/jgeosci.335

Original paper

Cronstedtite from Litošice, Czech Republic

Jiří HYBLER[1]*, Zdeněk DOLNÍČEK[2], Jiří SEJKORA[2]

[1] *Institute of Physics, Czech Academy of Sciences, Na Slovance 2, CZ-182 21 Praha 8, Czech Republic; hybler@fzu.cz*
[2] *Department of Mineralogy and Petrology, National Museum, Cirkusová 1740, CZ-193 00 Praha 9, Czech Republic*
[*] *Corresponding author*

The layered iron silicate cronstedtite was encountered in ore veins in the exploration shaft mined in the Neoproterozoic black shale-hosted pyrite-manganese deposit near Litošice (Eastern Bohemia, Czech Republic) around 1955. It forms up to 2 mm thick black double or single bands in symmetrically zoned hydrothermal veins cutting shales. The specimens selected from available material were studied by single-crystal X-ray diffraction using the four-circle diffractometer with an area detector. The chemical composition of some of the specimens was determined by the electron probe microanalysis (EPMA) in the WDS mode. Furthermore, a polished section of the ore material with cronstedtite bands was prepared, and the mineral association was analyzed with the aid of back-scattered electron (BSE) images. The interpretation of reciprocal space (RS) sections produced by the diffractometer software allowed the determination of OD subfamilies (Bailey's groups) A, B, C, D, and polytypes. The 1*T* polytype (subfamily C), $a = 5.52$, $c = 7.12$ Å, space group $P31m$, is the most abundant in the occurrence. In rare cases, it forms oriented crystal associations (allotwins) with the 1*M* polytype (subfamily A), $a = 5.52$ Å, $b = 9.55$, $c = 7.136$ Å, $\beta = 104.4°$, space group Cm. Fully disordered allotwinned crystals of the A+C subfamilies were found, too. In addition, few allotwins of the polytype $2H_1$ (subfamily D) with a small amount of $2H_2$, were identified. Unit cell parameters are $a = 5.49$, $c = 14.21$ Å, space groups are $P6_3cm$ ($2H_1$), and $P6_3$ ($2H_2$). EPMA-WDS of selected crystals of prevailing 1*T* polytype revealed elevated contents of Mn (0.19–0.62 *apfu*) and low contents of Mg (up to 0.13 *apfu*) and Cl (up to 0.05 *apfu*), respectively. More rare $2H_1$ ($+2H_2$) polytypes show elevated contents of Mg in the range of 0.19–0.62 *apfu* and distinctly lower Mn (up to 0.07 *apfu*) and Cl contents (up to 0.01 *apfu*). The BSE images reveal that cronstedtite bands are associated with multiple generations of carbonates (rhodochrosite, siderite, rarely magnesite and calcite), quartz, opal, pyrite and carbonate-fluorapatite. Intense metasomatic replacement of cronstedtite by opal and siderite appeared especially around the center of the studied vein.

Keywords: Cronstedtite, 1 : 1 layered silicate, polytypism, stacking disorder, allotwinning
Received: 30 July 2021; accepted: 9 December 2021; handling editor: J. Kotková
The online version of this article (doi: 10.3190/jgeosci.335) contains supplementary electronic material.

1. Introduction

The layered silicate cronstedtite is 'Grandfathered' mineral first described by Steinmann (1820, 1821) from the Vojtěch Mine in Příbram, and named in honor of the Swedish chemist and mineralogist Axel Fredrik Cronstedt (*23. 12. 1722, †19. 8. 1765). It was subsequently described from Rejské Lode in the Kaňk part of the Kutná Hora ore district by Vrba (1886), and more recently by Novák et al. (1957). Other occurrences reported in the Czech Republic are Chvaletice (Novák and Jansa 1965; Hybler 1998), Pohled Quarry near Havlíčkův Brod (Hybler et al. 2016), Chyňava (Fiala 1951; Fiala and Kouřimský 1980; Hybler and Sejkora 2017), and Litošice (Novák and Hoffman 1956; Hybler 1998, this study). Several other occurrences in Central Europe were also reported: Rožňava (Varček et al. 1990), Nižná Slaná (Hybler et al. 2017) in Slovakia, Nagybörzsöny in Hungary (Hybler et al. 2020), and Lutherstadt Eisleben in Germany (Hybler 2014). Generally, cronstedtite is a scarce mineral, as it was usually found in a limited amount and/or in a limited time window. Some occurrences are quite unique – like a piece of a drill core from the Chyňava borehole, or a few pieces of the ore material found in a veinlet in the Pohled Quarry, quickly removed by a continuing excavation.

Cronstedtite typically occurs in low- and medium temperature hydrothermal veins together with quartz, calcite, in some cases with siderite, ankerite, rhodochrosite, and/or rhodonite, but always with pyrite – on the surface, in cavities, druses, inter-grown, in veinlets, or embedded in the polycrystalline mass or weathering products (e.g., Hybler et al. 2016, 2017). It has also been found in metamorphic banded iron formations (Gole 1980a, b; López-García et al. 1992), and in some meteorites, such as CM chondrites (e.g., Müller et al. 1979; Barber 1981; Burbine and Burns 1994; Browning et al. 1996; Lauretta et al. 2000; Zega and Buseck 2003; Schulte and Schock 2004; Dyl et al. 2010; Pignatelli et al. 2016, 2017, 2018). Spectroscopic data suggest that cronstedtite might be present in extraterrestrial environments, such as certain dark regions of Mars (Calvin 1998) and on the dwarf

planet Ceres (Zolotov 2014). Pignatelli et al. (2013, 2020) repeatedly synthetized micrometer-sized crystals of cronstedtite by an iron–clay reaction at 60–90 °C. Samples from these syntheses were later studied by Hybler et al. (2018) by electron diffraction.

Cronstedtite belongs to 1 : 1 phyllosilicates of the serpentine–kaolinite group (Steadman and Nuttall 1963, 1964; Steadman 1964). Its structural formula is $(Fe^{2+}_{3-x}Fe^{3+}_{x})(Si_{2-x}Fe^{3+}_{x})O_5(OH)_4$, where x is usually in the range of 0.5 to 0.85. The structure is composed of edge-sharing octahedral and adjacent corner-sharing tetrahedral sheets, forming together 1 : 1 layer (Bailey 1988). Octahedral positions are occupied by Fe^{2+} and Fe^{3+}, while Si^{4+} is partially substituted by Fe^{3+}in tetrahedral positions. Presumably, the proportion of Fe^{3+} in octahedra balances the charge deficiency in tetrahedra. Moreover, a partial substitution of Fe^{2+} in octahedra for Mn^{2+} and/or Mg^{2+} has been reported in cronstedtite from some occurrences, e.g., Příbram (Steinmann 1821; Damour 1860; Janovský 1875; Geiger et al. 1983), Chyňava and Ouedi Beht, Morocco (Hybler and Sejkora 2017; Hybler et al. 2021). The Mn-rich analog of cronstedtite described from South Africa was approved as a new distinct mineral species guidottiite (Wahle et al. 2010).

The 1 : 1 layer silicates, including cronstedtite are typical representatives of Order-Disorder structures of layers (OD structures in the following text) with a low degree of desymmetrization (Dornberger-Schiff and Ďurovič 1975a, b; Ďurovič 1981, 2004). They belong to the OD family, subdivided into four OD subfamilies according to shifts and/or rotations of consecutive (identical) layers. These subfamilies are identical to Bailey's (1969, 1988) groups: A (polytypes 1*M*, $2M_1$, 3*T*, $6T_2$), B (2*O*, $2M_2$, 6*H*), C (1*T*, 3*R*, 2*T*) and D ($2H_1$, $6R_1$, $2H_2$). The stacking rules are represented by the following operations: $\pm\mathbf{a}_i/3$ shifts for subfamily A, $\pm\mathbf{a}_i/3$ shifts combined with 180º rotation for subfamily B, $\pm\mathbf{b}/3$ or no shift for subfamily C, $\pm\mathbf{b}/3$ or no shift combined with 180º rotation for subfamily D, where $\mathbf{a}_i$, $\mathbf{b}$ correspond to the vectors of trigonal and orthohexagonal cells, respectively. Such variability of layer stacking gives rise to a relatively high amount of polytypes.

Groups and polytypes are identified with the aid of characteristic single-crystal X-ray diffraction patterns, Selected Area Electron Diffraction (SAED), and Electron Diffraction Tomography (EDT). The X-ray powder diffraction is not reliable in many cases for the polytype determination (Ďurovič 1997).

Existing single-crystal diffraction data for several cronstedtite samples from Litošice using the precession camera resulted in the identification of only 1*T* polytype (Hybler 1998). Later studies of cronstedtite from other localities (Hybler and Sejkora 2017; Hybler et al. 2016, 2017, 2020) manifested the necessity of checking a large number of specimens (tens or even hundreds) by single-crystal X-ray diffraction in order to reveal possible variability.

The aim of this study is to provide detailed data on the mineral cronstedtite using samples stored in the National Museum, Prague, which have become available for research. In particular, it focuses on testing more specimens for polytypism, twinning, allotwinning and stacking disorder, which might be present within one occurrence, along with the determination of the chemical composition, paragenesis and relations to other minerals in the assemblage.

2. Occurrence

2.1. Geology

Neoproterozoic stratiform Mn-carbonate and pyrite mineralization of "black shales" occurs in a disjunctively disturbed synclinorium in the Chvaletice–Zdechovice–Morašice–Litošice–Sovolusky belt in the Železné hory, Proterozoic Unit (Central/Eastern Bohemia, Czech Republic). The mineralization has been interpreted as a product of submarine volcanic activity and is partly affected (especially in the SE part) by metamorphic processes (Bernard 1991). The prevailing stratiform ore mineralization is accompanied by younger veins with a high content of Mn. The Fe and Mn ores were mined on a small scale in this area from the Middle Ages, and the main deposit Chvaletice was exploited as a source of pyrite for the chemical industry by a large open-pit mine in 1951–1975. More than 30 million tons of pyrite ores were produced (Bernard 1991).

2.2. Mining history and mineralogy

Litošice is a small village on the boundary of Central and Eastern Bohemia, about 7 km SSW of Přelouč, 20 km SW of Pardubice. The approximately 500 m wide ore zone strikes in NW–SE direction, starting 1 km W of Litošice and terminating 0.5 km SW of Sovolusky. It is largely covered by forest except for its SE margin. This zone represents a southeastern continuation of the Chvaletice deposit.

In the study of Slavík (1928) and unpublished research reports of Kempný et al. (1955) and Bartas (1960), the mining activities were reported south of the road Litošice–Žehušice, i.e., 1.2 km W of Litošice, in 1916–1917, 1919 and 1930. The 53 m deep shaft with four levels and numerous adits was opened in 1919 or 1920 by the Prague Iron Company in this area. Moreover, remnants of even older mining activity (depressions, slumps) were apparent nearby, too. They were probably

excavated for "*limonite*" from a gossan since the Middle Ages. Slavík (1928) also reported two quarries near Sovolusky and Morašice opened in 1926 and 1927. Bartas (1960) mentioned two smaller shafts SW from Sovolusky, 18 m and 11 m deep, respectively. All these workings were exploited for the manganese ores. Following minerals were reported in the study of Slavík (1928) for the Litošice area: pyrite, pyrrhotite, garnet, amphibole asbestos, arsenopyrite, chalcopyrite, quartz (colorless or in the form of amethyst), manganite, hausmannite, calcite, rhodochrosite, siderite, alunite, destinezite, aluminite, delvauxite, vivianite, vashegyite, anthophyllite, and alone curious discovery of anthracite. The genesis of Litošice and other deposits in the area was described by Slavík (1929). In the 1950s, an extensive geological exploration for pyrite mineralization in black shales was performed. These workings, geological mapping and drilling, were carried out from 1952 by the Central Geological Institute (Ústřední Ústav Geologický), Prague. From 1954, the Czech–Moravian Ore Research (Českomoravský rudní průzkum), Kutná Hora continued in explorations by boring of denser network of boreholes and digging of shafts 10, 11, 13, 14, 15, 16. While only short galleries were driven from the shafts 13, 14, 15, extensive networks of adits on two levels were advanced from the shafts 10, 11 and 16. The aim of these explorations was the verification of reserves of pyrite shales in the deposit for the exploitation planned after the closure of the nearby Chvaletice quarry. Several reports of these exploration works are stored in the Czech Geological Survey – Geofond, Prague: Bartas (1955, 1960), Kempný et al. (1955), Fiala and Svoboda (1953, 1956), Papoušek (1956a, b, 1957). The reports of Bartas (1955, 1960) are the most comprehensive, containing numerous drilling profiles as well as the geological map of adits dug on two levels (at 50 and 100 m depth) from shaft No. 10. The entire geological profile of excavation of shaft No. 10 is included in the report of Kempný et al. (1955). A rhodochrosite vein in the depth of 41–45 m, 50 cm thick, striking NW–SE and dipping 58–66° to NE was encountered during the digging of the shaft. Bartas (1960) reported two rhodochrosite veins encountered in the heading denoted as 101 (depth 50 m), in direction SE 1–3 m and 18–20 m far from the shaft, respectively. Another thin rhodochrosite vein was also observed at cross adits denoted as 1001 and 1002 around the shaft.

Since pyrite used for the production of sulfuric acid was gradually replaced by the import of native sulfur from Poland since the late '50s, the deposit was never exploited and remained as a reserve. At present, the shafts are abandoned, filled up with formerly excavated material and remains of dismantled dumps. Žák (1955) studied material from the shaft (as stated in the study) 1200 m S of Litošice, evidently corresponding to shaft No. 10. He explored material from the ore vein at a depth of 41–45 m. Alabandite (2 generations), accompanied by other minerals: rhodochrosite (4 generations), neotokite, pyrite, ankerite, quartz, chalcedony, was reported. No cronstedtite was reported.

Novák and Hoffman (1956) described several minerals from the material collected in the area. They also explored a dump of the shaft near Sovolusky (as they reported) – evidently of shaft No 10. The authors described samples with symmetrical bands of black cronstedtite of the thickness up to 5 mm along with carbonate–rhodochrosite vein with quartz in the center. Qualitative spectral and wet chemical analyses revealed a certain content of Mn. However, they attributed it to a possible admixture of rhodochrosite. The powder diffraction data were reported and compared with data of cronstedtite from Kutná Hora and Cornwall. No attempt to perform single-crystal studies was made. Other minerals reported from this shaft are opal, alabandite, neotokite, and pyrite.

Cronstedtite was later recognized in the material collected by Lubor Žák (LŽ) in 1955, originating from the shaft No. 10, the ore vein at a depth of 41–45 m (LŽ, priv. comm.). Hybler (1998) presented the first preliminary single-crystal diffraction study of cronstedtite from Litošice (obtained directly from LŽ) and nearby Chvaletice using the precession camera. He identified nothing but the 1*T* polytype in a few samples from Litošice he studied at that time.

3. Samples

Small fragments of ore material provided by LŽ to the first author of this paper (JH), and several compact pieces of carbonate veins with bands of cronstedtite stored in the collection of the National Museum were used for this study. All samples with their catalog numbers, donators, and brief characteristics are reported in Tab. 1. With one exception, all of them evidently originated from the shaft No. 10 (GPS 49°58'23.8"N, 15°30'38.7"E); however, the reported localities are distinct – Litošice, Sovolusky, Semtěš, and Vápenka. The reason for this ambiguity, also found in the studies cited above, is the location of the shaft at comparable distances from given villages and places. However, shaft No. 10 is located in the cadastral area of Litošice. Thus this name is used for the locality in the following text.

Note that two samples donated by LŽ (P1N 111848 and P1N 111849), collected in 1955, are explicitly attributed to shaft No. 10, depth of 47 m. The sample P1N 111848 is presented in Fig. 1. The other two well-localized samples came from the same shaft, depth of 50 m, first head (P1N 66872) or E–W-trending cross adit 15 m from the shaft (P1N 74127). The relationship

Fig. 1 Ore vein with symmetrically arranged black double bands of cronstedtite. National Museum, Prague, catalog number P1N 111848. Photo P. Škácha.

between these occurrences around shaft No. 10 cannot be assessed. Cronstedtite usually forms double, rarely single bands about 5 mm thick, symmetrically located on both sides of the core of the vein, composed of opal and Fe–Mn carbonates. It is black colored, with vitreous luster and with perfect {001} cleavage.

The last listed sample is originally from the collection of Karel Paděra cat. No. P1N82054 is initially labeled as Morašice. The sample's appearance and other characteristics (polytypes, chemical compositions) are similar to the other samples. However, the given village is relatively far from shaft No. 10 (3.2 km). Thus the sample possibly comes from another locality. In the proximity of Morašice, two mining works are referred to in the Czech Geological Survey – Geofond: an old, pre-1945 adit (49°59'51.5"N, 15°29'10.3"E), and a post-WWII shaft No. 52 (50°00'25.9"N, 15°28'36.6"E). Nevertheless, we assume that the described sample comes from Litošice, too, as this ore district was previously referred to as Zdechovice–Morašice (Bernard et al. 1981), and localization of samples from the Paděra's collection is often not too accurate.

4. Experimental techniques

Crystals were separated from bands in the given samples and under the stereomicroscope. The typical size of specimens was 0.05–0.2 mm. Separated fragments were labeled according to the catalog numbers of samples, like P1N40571-1, P1N40571-2, etc. In the case of the P1N 111848 sample, several batches of fragments were taken from individual sequentially labeled bands, with two

Tab. 1 List of samples used for the study.

Origin*	Catalogue Number	Locality quoted	Donated by	Form	Fragments studied
LZ		Litošice – shaft No. 10, dump	Lubor Žák, personally to JH	fragments	46
NM	P1N 40571	Litošice – shaft No. 10	Lubor Žák	bands in carbonate vein	18
NM	P1N 52382	Sovolusky – shaft No. 10	Vl. Hofman, Kutná Hora	bands in carbonate vein	35
NM	P1N 60314	Litošice	J. Hora, Prague	bands in carbonate vein	6
NM	P1N 66872	Vápenka near Semtěš – shaft No. 10, carbonate vein on the 1. heading	P. Povondra, Prague	bands in carbonate vein	9
NM	P1N 74127	Semtěš – "Na vápence", shaft No. 10, E-W cross adit 15 m from the shaft	J. V. Frič, Prague	bands in carbonate vein	23
NM	P1N 111848	Litošice – Vápenka, shaft No. 10, depth 47 m, 1200 m S from Litošice	Lubor Žák, Prague (in 2006, collected 1955)	bands in carbonate vein	35
NM	P1N 111849	Litošice – Vápenka, shaft No. 10, depth 47 m, 1200 m S from Litošice	Lubor Žák, Prague (in 2006, collected 1955)	bands in carbonate vein	none
NM	P1N 82054	Morašice	Karel Paděra, Prague	bands in carbonate vein	24

* LZ – obtained directly from Lubor Žák; NM – collection of the National Museum, Prague

batches representing two domains of band 3. The batches were thus labeled as P1N111848-V1, P1N111848-V2, P1N111848-V3H, P1N111848-V3S, and P1N111848-V4. All fragments were glued onto the glass fibers. They were studied by X-ray diffraction and some of them were afterward used for the electron probe microanalysis (EPMA).

4.1. Single crystal X-ray diffraction

Selected crystal fragments were studied by the single-crystal X-ray diffraction with the aid of the four-circle (double-wavelength) X-ray diffractometer Gemini A Ultra (Rigaku Oxford Diffraction) equipped with the CCD area detector Atlas S2 at the Institute of Physics, Czech Academy of Sciences. The MoK_α radiation, with graphite monochromator, λ = 0.71070 Å, and Mo-enhance fiber optics collimator were used. At the beginning of the study, special pre-experiments were performed covering a sufficiently large portion of the reciprocal space. Later the strategy was changed: the quick pre-experiment was performed first, followed by a complete experiment with limited parameters (mainly exposure time), but always covering the whole sphere. Such an experiment typically required tens of minutes or several hours. The CrysAlisPro version 171.41.93a (Rigaku Oxford Diffraction 2021) package was used for the data collection, unit cell parameters calculation, and processing of data recorded. A total of 196 specimens were tested. Some of them were later cleaved into smaller fragments, which were studied separately. About 380 frames were recorded during special pre-experiments and 500–600 frames during full experiments. The "*unwarp*" procedure created user-defined images of reciprocal space sections (RS sections in the following), which are equivalents of precession photographs.

The RS sections corresponding to six important reciprocal lattice planes were generated: $(2h\bar{h}l_{hex})^*$, $(hhl_{hex})^*$, $(\bar{h}2hl_{hex})^*$, $(h0l_{hex})^*$, $(0kl_{hex})^*$, and $(\bar{h}hl_{hex})^*$. Distributions of so-called subfamily reflections along the reciprocal lattice rows $[2\bar{1}l]^*$ / $[11l]^*$ / $[\bar{1}2l]^*$ in $(2h\bar{h}l_{hex})^*$ / $(hhl_{hex})^*$ / $(\bar{h}2hl_{hex})^*$ planes, respectively, are used to determine OD subfamilies (Bailey's groups) A, B, C, D (Dornberger-Schiff and Ďurovič 1975a, b; Bailey 1969; 1988). Similarly, distributions of characteristic reflections along $[10l]^*$ / $[01l]^*$ / $[\bar{1}1l]^*$ rows in $(h0l_{hex})^*$ / $(0kl_{hex})^*$ / $(\bar{h}hl_{hex})$ RS sections were used to determine polytypes. Graphical identification diagrams for a simple visual comparison with real diffraction patterns were used. They were already published elsewhere (Mikloš 1975; Ďurovič 1981, 1997; Weiss and Kužvart 2005; Hybler et al. 2018, 2021). Unit cell parameters of selected samples are summarized in Tab. 2. For some specimens, the full

Tab. 2 Unit-cell parameters (in Å, degrees, with standard uncertainties – s.u.'s in parentheses), subfamilies (Bailey's groups), and polytypes of selected crystals of cronstedtite from Litošice.

Sample	*a*	*b;* β	*c*	*V*	Group	Polytype(s)	Note
LZ-12-2	5.5162(6)	5.5162(6)	21.334(2)	562.19(11)	C+A	disordered	Disordered, diffuse streaks, cell parameters of the subfamily A structure, Fig. 5
LZ-14	5.5290(12)	5.5290(12)	7.1262(15)	188.66(7)	C	1*T*	Diffusely streaked, EPMA
LZ-23	5.5262(12)	5.5262(12)	7.124(2)	188.40(9)	C	1*T*	Diffusely streaked, EPMA
LZ-27	5.5264(16)	5.5264(16)	7.151(3)	189.15(12)	C+A	1*T*+1*M*	Allotwin, diffusely streaked, cell parameters 1*T* polytype
	5.5166(11)	9.5546(17); 104.44(2)	7.3585(17)	375.62(13)	C+A	1*T*+1*M*	Cell parameters 1*M* polytype, Fig. 4
LZ-40	5.5263(13)	5.5263(13)	7.1288(18)	188.54(8)	C	1*T*	Diffuse streaks, EPMA
LZ-41	5.5200(12)	5.5200(12)	7.119(2)	187.86(8)	C	1*T*	Diffuse streaks, parasitic misoriented crystals, EPMA
LZ-44	5.5181(15)	5.5181(15)	7.127(2)	187.94(9)	C(+A?)	1*T*	Subfamily A reflections weak, EPMA
P1N 40571-3	5.529(2)	5.529(2)	7.182(4)	190.16(15)	C	1*T*	Char refl. weak, smeared, diffuse streaks, EPMA
P1N 40571-9	5.4942(5)	5.4942(5)	14.2146(13)	371.60(6)	D	$2H_1$+($2H_2$)	Allotwin, strong $2H_1$, weak $2H_2$ reflections, diffuse streaks, EPMA, Fig. 3
P1N 40571-13	5.5211(8)	5.5211(8)	7.1368(12)	188.40(5)	C	1*T*	Diffuse streaks, EPMA, Fig. 2
P1N 60314-2	5.552(5)	5.552(5)	7.069(9)	188.9(3)	C	1*T*	Poor crystal, char. refl. weak, diffuse streaks, EPMA
P1N 60314-4	5.545(2)	5.545(2)	7.130(2)	189.89(13)	C	1*T*	Char. refl. weak, diffuse streaks, Debye arcs, EPMA
P1N 60314-6	5.5195(9)	5.5195(9)	7.1292(14	188.09(6)	C	1*T*	Characteristic reflections strong, diffuse streaks
P1N 74127-9	5.5248(9)	5.5248(9)	7.1444(16)	188.86(6)	C	1*T*	Characteristic reflections strong, diffuse streaks
P1N 111848-V2-3	5.5176(10)	5.5176(10)	7.1233(16)	187.81(6)	C	1*T*	Characteristic reflections strong, diffuse streaks, Debye arcs, EPMA
P1N 111848-V4-6	5.5170(6)	5.5170(6)	7.1377(10)	188.15(4)	C	1*T*	Average cryst., char. refl. aver., diffuse streaks, Debye arcs, EPMA
P1N 82054-1	5.516(2)	5.516(2)	7.137(4)	188.06(15)	C	1*T*	Reportedly from Morašice? EPMA

EPMA – sample selected for EPMA, LZ – samples from Lubor Žák, other samples from National Museum

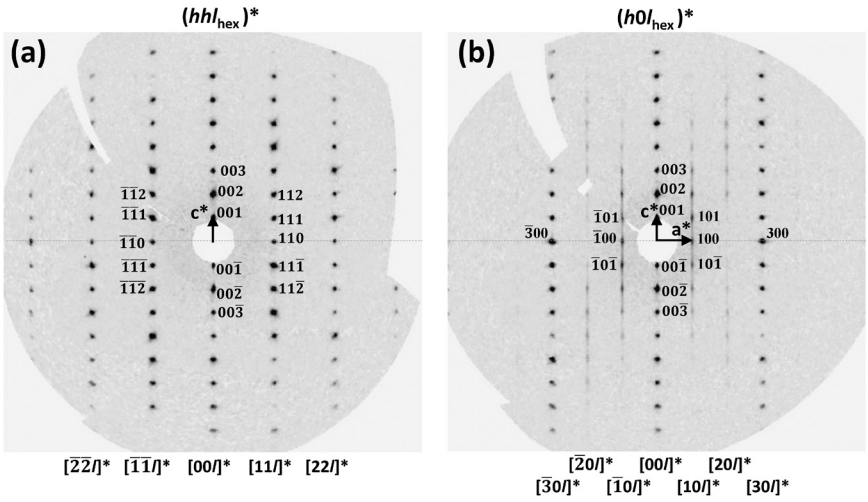

Fig. 2 RS sections – equivalents of precession photographs of the polytype 1*T*. Indices of reciprocal lattice rows and of selected reflections, as well as reciprocal lattice vectors are indicated where possible. Auxiliary horizontal lines passing through the origins of sections are added to aid the eye in all RS section images presented in this study. **a** – The $(hhl_{hex})^*$ section. The reflections of [11*l*]*, and symmetry equivalent [$\bar{1}\bar{1}l$]*, reciprocal lattice rows are at the same levels as reflections of the [00*l*]* row. This arrangement is characteristic for the subfamily C. **b** – The $(h0l_{hex})^*$ section with characteristic reflections [10*l*]* and [$\bar{1}$0*l*]*, also at the same level as reflections of the [00*l*]* row, characteristic for the 1*T* polytype. The same is valid also for second-order characteristic rows [20*l*]* and [$\bar{2}$0*l*]*. Note smeared and diffusely streaked characteristic reflections due to partial stacking disorder. Specimen P1N 40571-13.

experiment was repeated with modified parameters in order to obtain more precise and less noisy RS sections for the publication.

4.2. Electron probe microanalysis

The selected fragments of cronstedtite crystals (30 fragments from 8 samples), in which polytypes were determined, were mounted in epoxy discs and polished by diamond suspensions. In addition, one polished section was prepared from a slab taken from the bulk vein with cronstedtite bands of the sample P1N74127 to assess the whole mineral paragenesis. After inspection under a polarizing microscope, samples were coated with a carbon layer of about 30 nm in thickness and analyzed at the National Museum in Prague, using a CAMECA SX-100 electron probe microanalyzer. Identification of minerals based on rapid energy-dispersive spectra (EDS) was followed by quantitative measurements of chemical composition of selected phases in the wavelength-dispersive (WDS) mode with an acceleration voltage of 15 kV, beam current of 10 nA (apatite, cronstedtite) or 5 nA (carbonates) and beam diameter of 5 μm. The following elements were analyzed in individual mineral phases: *cronstedtite*: Al, Ca, Cl, F, Fe, K, Mg, Mn, Na, P, S, Si, Zn; *carbonates* and *SiO_2 minerals*: Al, Ba, Ca, Co, Fe, Mg, Mn, Na, Ni, P, S, Si, Sr, Zn; *apatite*: Al, As, Ba, Ca, Ce, Cl, F, Fe, K, Mg, Mn, Na, P, Pb, S, Si, Sr, Y and Zn. The following standards and analytical lines were used: albite (NaK_α), baryte (BaL_α), $CePO_4$ (CeL_α), Co (CoK_α), chalcopyrite (CuK_α), clinoclase (AsL_β), fluorapatite (CaK_α, PK_α), celestite (SrL_β, SK_α), diopside (MgK_α), halite (ClK_α), hematite (FeK_α), LiF (FK_α), Ni (NiK_α), rhodonite (MnK_α), sanidine (KK_α, SiK_α, AlK_α), vanadinite (PbM_α), wollastonite (CaK_α), YVO_4 (YL_α) and ZnO (ZnK_α). The peak counting times were between 10 and 20 s and half of the peak time was used for both background positions. The raw counts were converted to wt. % using the standard PAP procedure (Pouchou and Pichoir 1985). Automatic correction of overlap CaK_β - PK_α in carbonate analyses was applied. Oxygen was calculated from stoichiometry. The above-listed elements, which are not included in the tables of primary data (Tabs S1–S3, ESM) were in all cases below the limits of detection. The contents of H_2O, Fe^{2+} and Fe^{3+}, as well as *x*-values, were calculated on the basis of the general formula of cronstedtite $(Fe^{2+}_{3-x}Fe^{3+}_x)(Si_{2-x}Fe^{3+}_x)O_5(OH)_4$.

5. Results and discussion

5.1. Polytypes found

Cronstedtite crystals from Litošice belong mostly to the 1*T* polytype. Unit cell parameters are $a = 5.52$, $c = 7.12$ Å, space group is $P31m$. It is the simplest polytype of the subfamily (Bailey's group) C, as it is built by the mere stacking of layers without any shift. This polytype is ubiquitous in all samples studied as well as in all bands. Almost all crystals exhibit partial stacking disorder. The characteristic reflections on RS sections are smeared, and diffuse streaks along reciprocal lattice rows are present. Well-ordered crystals providing sharp characteristic reflections are rare. Typical RS sections of partially disordered 1*T* polytype are presented in Fig. 2.

The polytype $2H_1$ (subfamily D) was identified in two crystals from the sample P1N 40571. Both crystals also

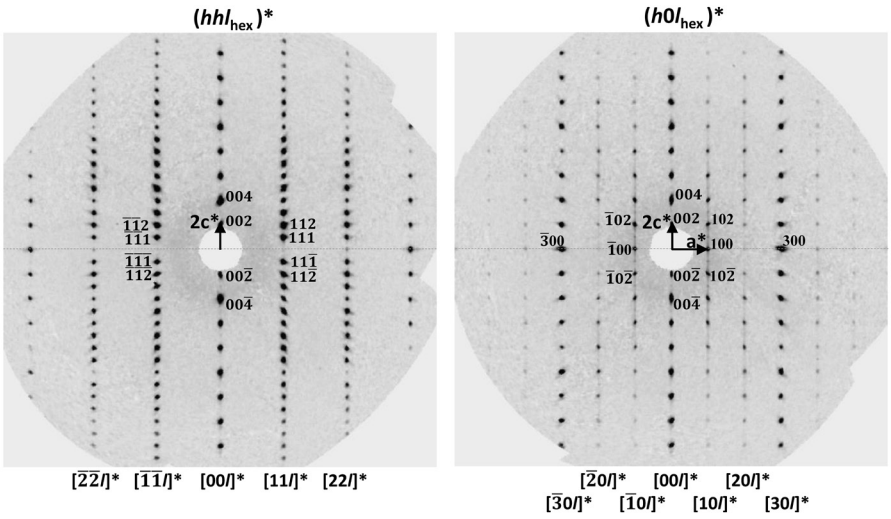

Fig. 3 RS sections of the polytype $2H_1$, with a small amount of the polytype $2H_2$, in fact, $2H_1$+$2H_2$ allotwin. Selected reflections are indexed and reciprocal lattice vectors are indicated when possible. **a** – The (hhl_{hex})* section, with reflections for the subfamily D in [11*l*]*, and [$\bar{1}$1*l*]* reciprocal lattice rows. Their periodicity is the half of [00*l*]* row, which means doubled periodicity in the direct space due to regular alternations of layers rotated by 180°. **b** – The $(h0l_{hex})$* section. Strong characteristic reflections [10*l*]* and [$\bar{1}$0*l*]* have the same periodicity as these of the [00*l*]* row, because the $l = 2n+1$ reflections are absent due to systematic absences of the space group $P6_3cm$. The weak $l = 2n+1$ reflections belong to the polytype $2H_2$, space group $P6_3$. Specimen P1N 40571-9.

contain a small amount of the polytype $2H_2$. For this kind of oriented crystal association of polytypes Nespolo et al. (1999) proposed the term allotwin. Unit cell parameters are a = 5.49, c = 14.21 Å, space groups are $P6_3cm$ ($2H_1$), and $P6_3$ ($2H_2$). The respective RS sections of one of such allotwins are shown in Fig. 3. The second selected specimen is very poorly crystalline.

Several rare crystals in the occurrence produced complex diffraction patterns containing the reflections of the subfamilies C and A. Moreover, in diffraction patterns of some of these crystals, the reflections of 1*T* as well as of the 1*M* polytypes were found. These crystals represent other examples of allotwins. While the 1*T* polytype is common in the occurrence, the 1*M* polytype (a = 5.52 Å, b = 9.55, c = 7.136 Å, β = 104.4°, space group *Cm*), belonging to the A subfamily was identified only in several specimens, and always as components of allotwins. Representative RS sections are presented in Fig. 4.

The reciprocal lattice rows [2$\bar{1}$*l*]* / [11*l*]* / [$\bar{1}$2*l*]* in $(2h\bar{h}l_{hex})$* / (hhl_{hex})* / $(\bar{h}2hl_{hex})$* planes (Fig. 4a) reveal superposition of reflections of the A group (shifted by +1/3 or –1/3 of the periodicity of reflections of the [00*l*]* row), and of the C group (with reflections at the same level as in the [00*l*]* row). One of $(h0l_{hex})$* / $(0kl_{hex})$* / $(\bar{h}hl_{hex})$* RS sections reveal characteristic reflections at the level of reflections of the [00*l*]* row. However, they contain a contribution of the 1*T* polytype, and that of the plane perpendicular to the symmetry plane (*m*) of the 1*M* polytype, i.e., the $(h0l_{mon})$* RS section (Fig. 4d). The characteristic reflections of both polytypes overlap. In other RS sections of this kind, reflections of both polytypes are separated; while the 1*T* polytype reflections are still in the same positions, the 1*M* polytype reflections belonging to the plane diagonal to the symmetry plane (*m*) are shifted by 1/3 or –1/3 of the periodicity of the [00*l*]* row (Fig. 4b–c). A similar allotwinned 1*T*+1*M* (A+C) crystal was identified by electron diffraction in the synthetic run product (Hybler et al. 2018) and in a meteorite – Cochabamba carbonaceous chondrite (Müller et al. 1979). RS sections of isolated polytype 1*M* were published by Pignatelli et al. (2013), Hybler (2014), and Hybler et al. (2018, 2020). While the 1*M* polytype is generally rare, the much more abundant polytype 3*T* from subfamily A was not identified in the studied samples.

Several A+C allotwinned crystals are entirely disordered. Diffraction patterns of one of such crystals are presented in Fig. 5. The rows of characteristic reflections are replaced by diffuse streaks due to the stacking disorder.

5.2. Chemical composition of cronstedite

In order to examine compositional variability of the studied cronstedtite polytypes, a total of 235 spot analyses from thirty selected fragments and 66 spot analyses from a polished section of sample P1N74127 with cronstedtite bands were collected. The complete data set of analyses is given in Tab. S1 (ESM). The BSE imaging suggests the compositional homogeneity of all studied fragments of cronstedtite crystals.

For a predominant 1*T* polytype, the calculated x-values in the general formula range between 0.69 and 0.86 (Tab. 3), and samples show characteristic elevated contents of Mn in the range of 0.19–0.62 *apfu* (Fig. 6a), while the contents of Mg are distinctly lower and do not exceed 0.13 *apfu* (Fig. 6b). The presence of Mn and/or Mg partially replacing Fe^{2+} in octahedra has been reported from some occurrences, e. g. Příbram (Steinmann 1821; Geiger et al. 1983), Chyňava (Hybler and Sejkora

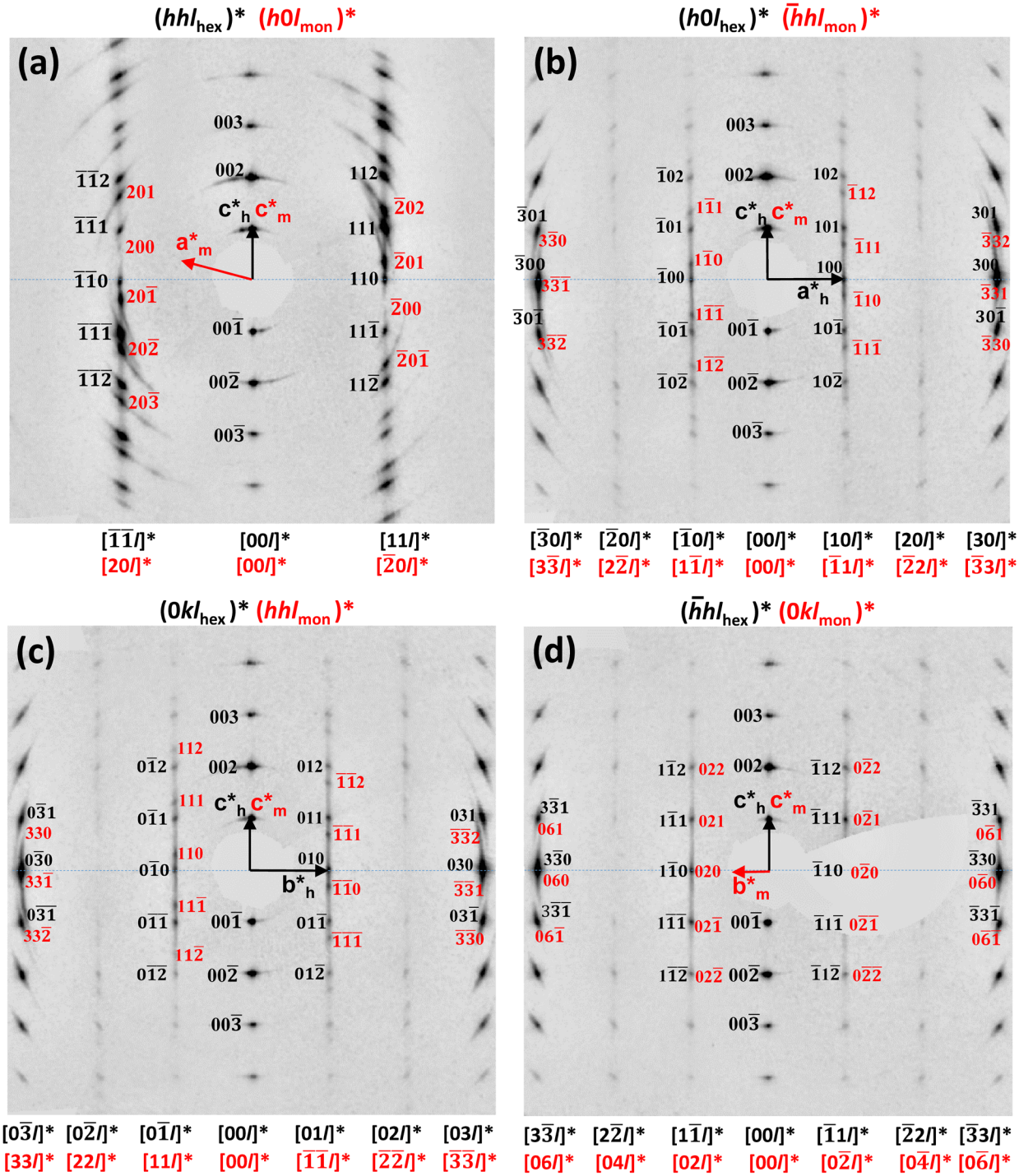

Fig. 4 RS sections of the rare allotwinned crystal of polytypes 1*T* and 1*M* of subfamilies C and A, respectively. Reciprocal lattice vectors are indicated where possible. (**a***$_h$, **b***$_h$ **c***$_h$ are hexagonal reciprocal vectors, **a***$_m$, **b***$_m$ **c***$_m$ are monoclinic reciprocal vectors). **a** – The superposition of (hhl_{hex})* and ($h0l_{mon}$)* RS sections 1*T* and 1*M* polytypes, respectively. The reflections of the subfamily C in [11*l*]* and [1̄1*l*]* rows (black indices) are at the same level as reflections of the of [00*l*]* row, while the reflections of the subfamily A in [20*l*]* and [2̄0*l*]* rows (red indices) are shifted by 1/3 **c*** c or –1/3 **c***. **b, c** – Superposition of the ($\bar{h}hl_{mon}$)* and (hhl_{mon})* RS sections, respectively, of the reciprocal lattice of the 1*M* polytype diagonal to the plane of symmetry and ($h0l_{hex}$)* and ($0kl_{hex}$)* sections, respectively, of the 1*T* polytype. The characteristic reflections of the 1*T* polytype (black indices) are at the same level as reflections of the [00*l*]* row, while the characteristic reflections of the 1*M* polytype (red indices) are shifted by 1/3 **c*** c or –1/3 **c***. **d** – Superposition of the RS section ($0kl_{mon}$)* of the reciprocal lattice of the 1*M* polytype perpendicular to the plane of symmetry and ($\bar{h}hl_{hex}$)* section of the 1*T* polytype. In this case, reflections of both polytypes are at the same level as reflections of the [00*l*]* row, and they thus overlap. Note also diffuse streaks along the rows of characteristic reflections due to partial stacking disorder and arc-shaped subfamily reflections due to poor crystallinity of the sample studied. Specimen LZ-27.

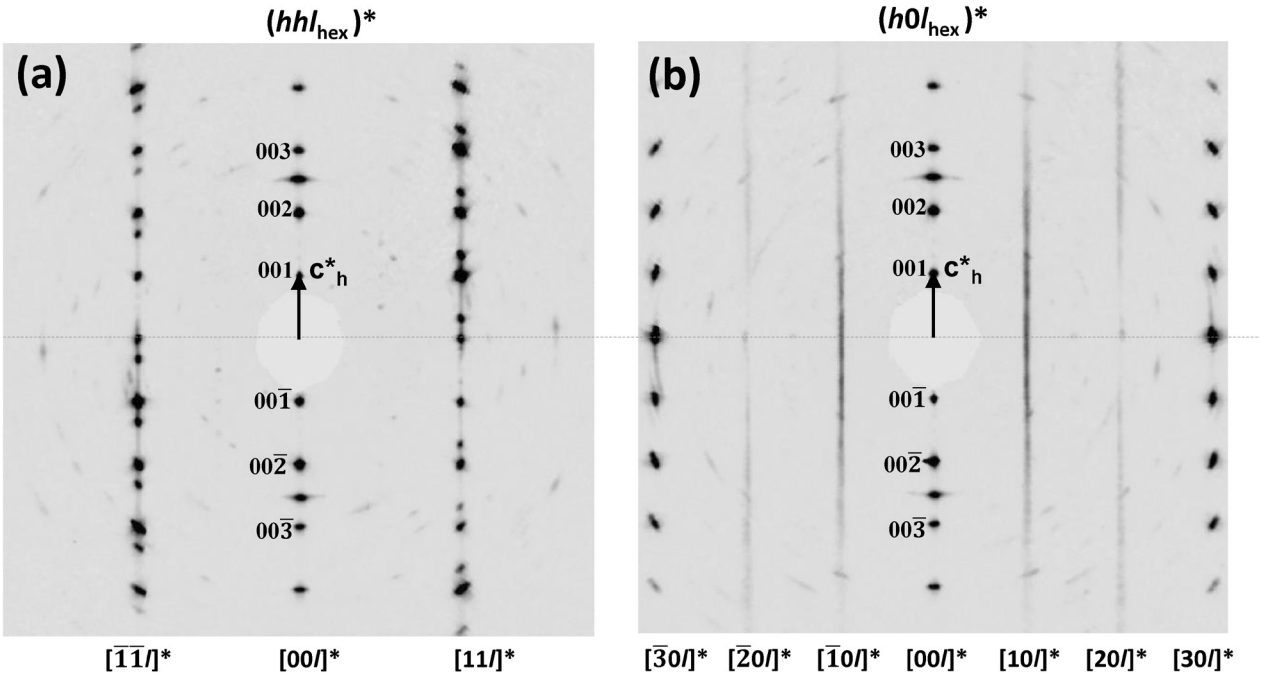

Fig. 5 RS sections of the rare disordered allotwinned crystal of subfamilies C and A. **a** – The (hhl_{hex})* RS section with reflections of C and A subfamilies like in Fig. 4a. **b** – The ($h0l_{hex}$)* section, with diffuse streaks instead of the characteristic reflections due to the stacking disorder. Specimen LZ-12-2.

2017) or Ouedi Beht, Morocco (Hybler et al. 2021). The Mn-analogue of cronstedtite, guidottiite, was described by Wahle et al. (2010) from 'N'Chwaning Mines, South Africa. The elevated contents of Cl in the range 0.02–0.05 *apfu* were also determined in the studied samples; these Cl contents are negatively correlated with Mn (Fig. 6c).

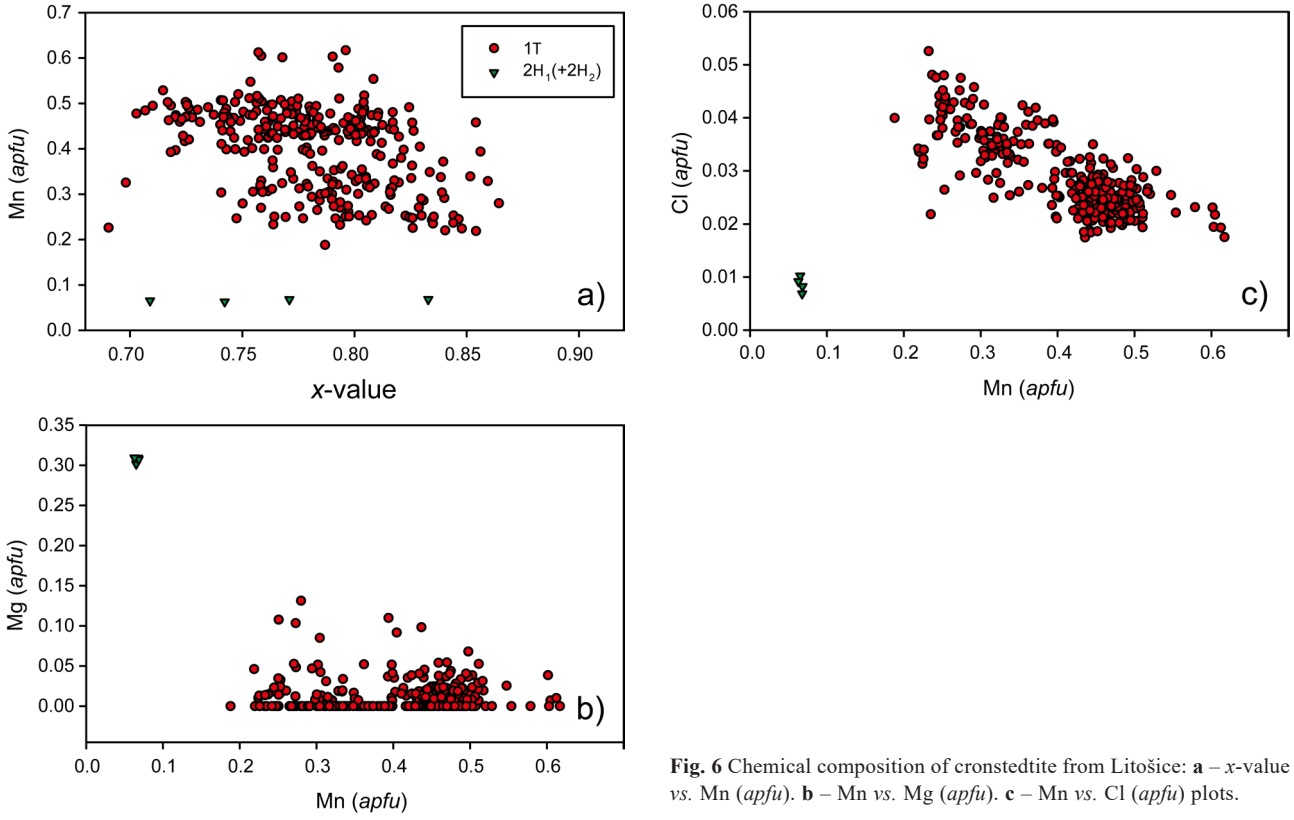

Fig. 6 Chemical composition of cronstedtite from Litošice: **a** – *x*-value *vs.* Mn (*apfu*). **b** – Mn *vs.* Mg (*apfu*). **c** – Mn *vs.* Cl (*apfu*) plots.

Tab. 3 Chemical composition of cronstedtite from Litošice (*apfu*).

sample	polytype		Fe^{2+}	Mg	Mn	Al	Fe^{3+}	Si	S	Cl	OH	*x*-value
LZ	1*T*	mean	1.774	0.006	0.438	0.001	1.564	1.217	0.002	0.024	3.974	0.78
		min	1.698	0.000	0.393	0.000	1.426	1.174	0.000	0.018	3.966	0.72
		max	1.889	0.036	0.493	0.010	1.653	1.282	0.006	0.030	3.982	0.83
P1N 111848	1*T*	mean	1.847	0.008	0.345	0.002	1.599	1.200	0.003	0.033	3.964	0.80
		min	1.678	0.000	0.219	0.000	1.486	1.146	0.000	0.017	3.942	0.74
		max	1.985	0.046	0.484	0.025	1.708	1.257	0.006	0.053	3.982	0.85
P1N 40571	1*T*	mean	1.887	0.006	0.319	0.002	1.576	1.211	0.003	0.034	3.963	0.79
		min	1.801	0.000	0.270	0.000	1.396	1.162	0.000	0.026	3.954	0.70
		max	1.977	0.034	0.350	0.015	1.677	1.302	0.005	0.044	3.972	0.84
P1N 52382	1*T*	mean	1.788	0.007	0.396	0.002	1.617	1.191	0.002	0.032	3.966	0.81
		min	1.674	0.000	0.298	0.000	1.557	1.175	0.000	0.025	3.958	0.78
		max	1.899	0.018	0.502	0.012	1.650	1.221	0.004	0.039	3.975	0.83
P1N 60314	1*T*	mean	1.732	0.013	0.492	0.008	1.518	1.237	0.002	0.024	3.975	0.76
		min	1.587	0.000	0.393	0.000	1.422	1.188	0.000	0.018	3.964	0.72
		max	1.819	0.039	0.617	0.037	1.617	1.283	0.004	0.032	3.982	0.81
P1N 66872	1*T*	mean	1.753	0.007	0.454	0.003	1.568	1.214	0.002	0.025	3.973	0.79
		min	1.717	0.000	0.438	0.000	1.489	1.174	0.000	0.021	3.969	0.74
		max	1.806	0.023	0.461	0.014	1.643	1.255	0.004	0.029	3.977	0.83
P1N 74127	1*T*	mean	1.845	0.003	0.356	0.001	1.590	1.204	0.003	0.035	3.963	0.80
		min	1.686	0.000	0.282	0.000	1.481	1.141	0.000	0.022	3.952	0.74
		max	1.948	0.031	0.486	0.014	1.719	1.259	0.006	0.046	3.976	0.86
P1N 74127 (PS)	1*T*	mean	1.811	0.027	0.395	0.009	1.525	1.233	0.002	0.030	3.968	0.77
		min	1.640	0.000	0.188	0.000	1.341	1.136	0.000	0.020	3.954	0.69
		max	2.084	0.131	0.516	0.075	1.729	1.310	0.006	0.042	3.980	0.86
P1N 82054	1*T*	mean	1.713	0.020	0.509	0.004	1.512	1.242	0.001	0.023	3.975	0.76
		min	1.607	0.000	0.441	0.000	1.429	1.207	0.000	0.019	3.966	0.71
		max	1.798	0.053	0.612	0.020	1.577	1.285	0.004	0.030	3.981	0.79
P1N 40571	$2H_1$(+$2H_2$)	mean	1.863	0.307	0.066	0.000	1.527	1.236	0.000	0.009	3.991	0.76
		min	1.792	0.302	0.063	0.000	1.418	1.167	0.000	0.007	3.990	0.71
		max	1.924	0.310	0.068	0.000	1.666	1.291	0.000	0.010	3.993	0.83

The presence of minor Cl in cronstedtite has been already known, e. g., from Pohled (Hybler et al. 2016), Chyňava (Hybler and Sejkora 2017), Nižná Slaná (Hybler et al. 2017), or Ouedi Beht (Hybler et al. 2021). Detectable contents of other elements were recorded only exceptionally (Al ≤ 0.08 *apfu*, S ≤ 0.01 *apfu*).

The chemical composition of the allotwin of $2H_1$ (+$2H_2$) polytypes (Tab. 3) differs significantly from the data of predominant 1*T* polytype (Fig. 6), especially by low Mn (0.06–0.07 *apfu*) and Cl (0.01 *apfu*) contents and an elevated content of Mg (up to 0.31 *apfu*). Calculated *x*-values in the range of 0.71–0.83 correspond to data of 1*T* polytype. Similar chemical composition was determined for $2H_2$ + $2H_1$ polytypes in the central part of a cronstedtite sample from Ouedi Beht (Hybler et al. 2021).

5.3. Cronstedite mineral association

Besides cronstedtite, sporadic carbonates and silica minerals replacing cronstedtite along the cleavage planes were recorded in fragments of cronstedtite used for the determination of polytypes (up to 0.2 mm in size). Carbonates, classified chiefly as siderite (Fig. 7), are chemically very heterogeneous among the individual samples ($Sd_{48–93}Rds_{0–38}Cal_{0–29}Mgs_{0–23}$). Rhodochrosite ($Rds_{97–98}Sd_{2–3}$; in sample P1N11848 only) and calcite ($Cal_{81–96}Sd_{3–17}$

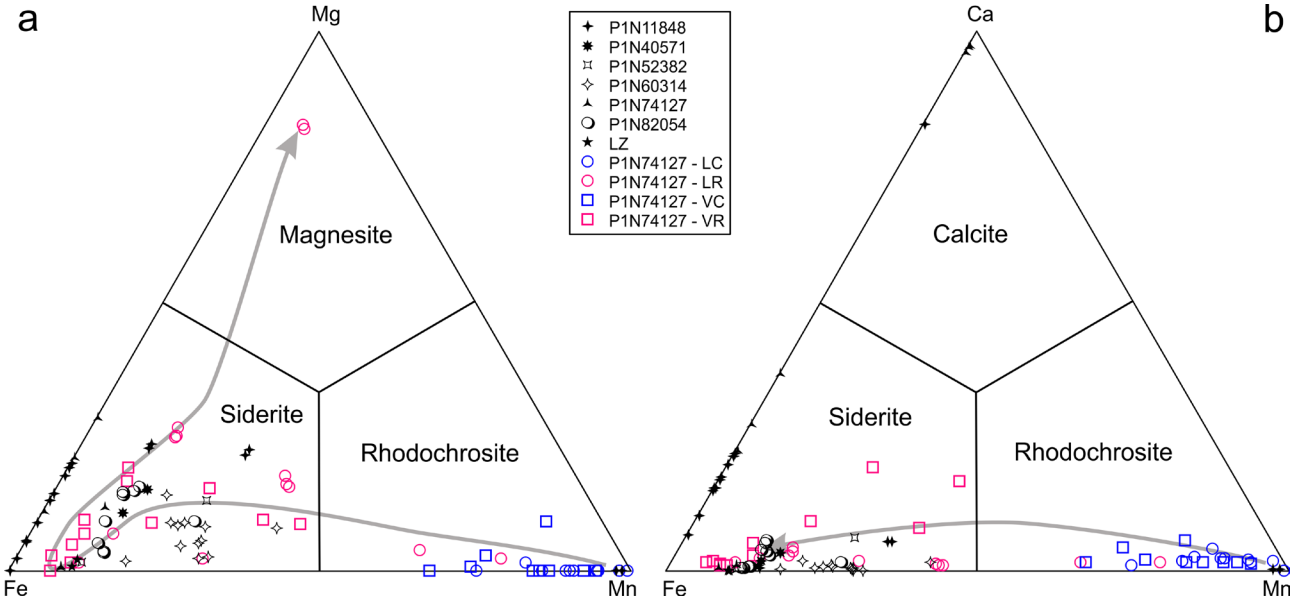

Fig. 7 Variability in the chemical composition of carbonates. **a** – plot Fe–Mg–Mn. **b** – plot Fe–Ca–Mn. The grey arrows indicate a general trend during the crystallization of carbonates. Note that calcite and magnesite data are not included in figures **a** and **b**, respectively. Abbreviations in legend: LC – layer core, LM – layer margin, VC – veinlet core, VM – veinlet margin.

$Mgs_{0–2}$; in samples P1N74127 and P1N11848) are less common than siderite. The minimal and fragmentary data due to the small size of these samples preclude any detailed interpretation of evolution during crystallization of carbonates.

The sample P1N74127 was selected for a detailed study of cronstedtite mineral association. It is formed by the symmetrically zoned vein about 1.5 cm thick. The vein consists of carbonates, cronstedtite, apatite, quartz, opal and pyrite. Zoning of the vein suggests repetitive open-space crystallization of main minerals, including Fe–Mn carbonates, opal and cronstedtite. The primary texture of the vein filling was modified by the processes of metasomatic replacement, especially around the central part of the vein.

Quartz and rhodochrosite, developed in the form of hemispherical aggregates with a layered texture defined by alternating layers of both minerals up to 0.5 mm thick (Fig. 8a), represent the early phases of the vein paragenesis. Quartz typically has a drusy character, being present in well-developed isometric crystals. Fine-grained rhodochrosite is chemically almost pure and exhibits no zonation in BSE images.

The remainder of the vein filling is composed of carbonates, cronstedtite and pyrite and contains several intercalations of opal instead of quartz. Opal typically forms botryoidal aggregates (Fig. 8b) and commonly also fine impregnations in the associated carbonates, as elevated Si contents indicate it in many of the WDS analyses (Tab. S2). Opal is chemically mostly pure, although the elevated contents of Fe, Mn and Mg in some analyses indicate an admixture of carbonates.

Cronstedtite forms two bands, each of about 2 mm in thickness, situated close to the central part of the vein and mutually separated by intercalations of Fe–Mn carbonate and opal (Fig. 8b). In BSE images, no chemical zoning was observed in cronstedtite aggregates. Cronstedtite is partly replaced by Fe-Mn carbonates along grain boundaries and cleavage planes (Figs. 8b–c). The intensity of this replacement increases towards the center of the vein, where apical parts of a younger cronstedtite layer are entirely replaced by aggregates of Fe–Mn carbonates and opal (Fig. 8d).

Cronstedtite and opal layers in the younger portion of the vein filling alternate with carbonate layers. Carbonates are dominated by siderite and rhodochrosite (Tab. S2), which exhibit similar texture and fabric in individual layers. The early massive fine-grained matrix typically evolves into elongated randomly oriented and mutually inter-grown branchy aggregates in the apical part of the layer (Figs 8b, e). The remaining open space in these porous parts was later wholly filled up by opal or pyrite (Fig. 8e). In BSE images, brighter cores of individual branches are rimmed by a darker outer rim (Figs 8b, e). Chemical composition evolves from rhodochrosite ($Rds_{74–99}Sd_{1–25}Mgs_{0–1}Cal_{0–4}$) to a chemically heterogeneous Fe/Mg-richer carbonate, which can be classified as Fe-rich rhodochrosite, Mn-rich siderite, siderite and/or Mg-rich siderite ($Rds_{10–77}Sd_{20–87}Mgs_{2–26}Cal_{1–3}$; Fig. 7). Identical chemical evolution is also observed for another morphological type of Fe-Mn carbonates present in thicker veinlets cutting and replacing cronstedtite (Figs 8b–c): a center of the vein is formed by rhodochrosite

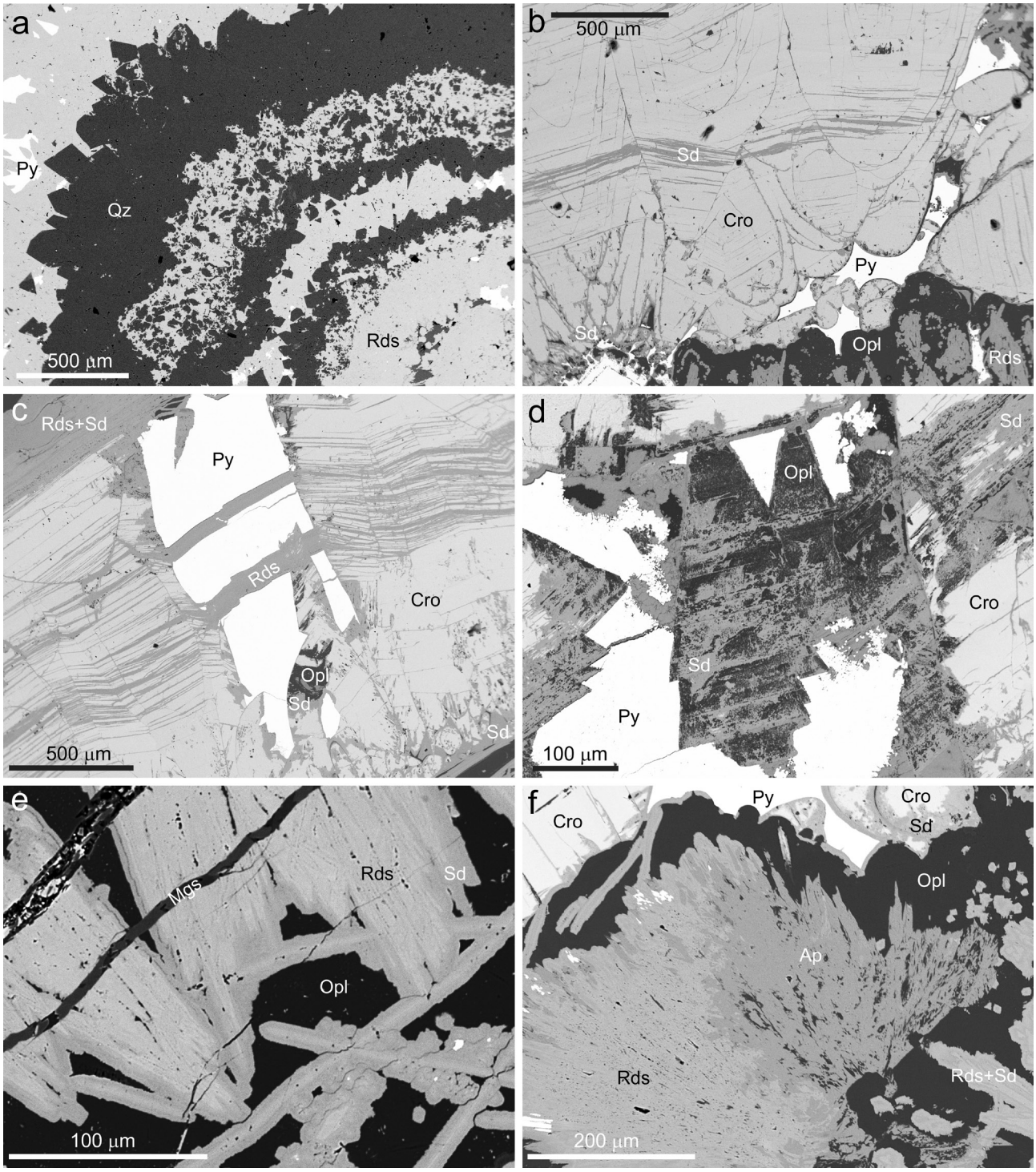

Fig. 8 Mineral paragenesis and texture of vein fill of the sample NM74127 on BSE images: **a** – the oldest portion of the vein fill, composed of fine layers of rhodochrosite (Rds), quartz (Qz) and minor pyrite (Py). **b** – branchy aggregates of rhodochrosite (Rds) overgrown by botryoidal opal (Opl) and followed by a thick layer of cronstedtite (Cro). The remaining open space in cronstedtite aggregate is fulfilled by pyrite (Py). Cronstedtite is weakly altered by siderite (Sd) along cleavage planes. **c** – example of more pronounced alteration of cronstedtite (Cro) by carbonates (Rds, Sd). **d** – youngest part of younger cronstedtite layer close to the center of the vein. In the central part of the figure, there is a cronstedtite grain which was entirely replaced by opal (Opl) and siderite (Sd), with still well visible cleavage planes of original cronstedtite in the pseudomorphosis. In the right part of the photograph, there are still preserved relics of cronstedtite in the carbonate matrix. **e** – growth zonality of branchy aggregates of Fe–Mg carbonates (Rds – rhodochrosite, Sd – siderite), surrounded by opal (Opl) and cut by younger veinlet of magnesite (Mgs). **f** – radial aggregate of apatite (Ap), partly replaced by rhodochrosite (Rds) and overgrown by botryoidal opal (Opl) and early cronstedtite layer (Cro). All photographs taken by Z. Dolníček.

($Rds_{66–93}Sd_{6–32}Mgs_{0–9}Cal_{1–6}$), and both margins by siderite to Mn-rich siderite ($Rds_{5–36}Sd_{41–92}Mgs_{0–18}Cal_{1–17}$; Fig. 7). By contrast, very thin veinlets are formed by siderite only. The textural evidence suggests that rhodochrosite was formed by crystallization in an open space (i.e., cementing open crack/fissure), whereas siderite originated by the replacement of cronstedtite. Thin veinlets of Fe-Mn carbonates are often present also in opal, but without signs of metasomatic replacement of this host mineral (Fig. 8e). Because of broad textural and chemical similarities/variations, the mutual temporal relationship of both major morphological types of Fe-Mn carbonates (primary precipitates in layers versus veinlets/replacements) remains unresolved. Magnesite ($Mgs_{81–82}Sd_{11–12}Rds_6Cal_{1–2}$) is a very rare carbonate. It forms either irregular small grains enclosed in opal, small overgrowths on Mn-rich siderite, or tiny veinlets in opal and primary layers of Fe-Mn carbonates (Fig. 8e). The general geochemical evolution during individual episodes of carbonate crystallization is uniformly characterized by the elemental sequence Mn → Fe → Mg (Fig. 7a). The Ca-richer (>8 mol. % of calcite molecule) carbonates are very rare, recorded only in a single spatially restricted domain.

Pyrite forms a filling of the remaining open space or veinlets in aggregates of cronstedtite and the primary layers of Fe-Mn carbonates. It predates veinlets of Fe-Mn carbonates replacing cronstedtite (Fig. 8c). Chemically, it does not contain admixtures at levels detectable by EDS spectra of the electron microprobe.

Apatite was observed only once. It forms a radial aggregate 0.4 mm in size predating an early layer of cronstedtite. The aggregate is overgrown and partly also consumed by Fe-Mn carbonates (Fig. 8f). WDS analyses showed significant admixtures of S and Mn and high contents of F (Tab. S3). A systematic deficit of elements in the position of phosphorus suggests the presence of elevated contents of CO_2 (Tab. S3), implying that the studied phase is carbonate-rich fluorapatite. Low analytical totals (97–98 wt. %; Tab. S3) may be associated with increased porosity due to the mechanism of formation of this mineral phase: specifically in the low-temperature sedimentary environment, there is presumed that crystallization of apatite would be a long-lasting process. Initially, an unstable gel-like non-stoichiometric calcium phosphate precipitates, which subsequently matured by water loss and stabilized by sorption of F and CO_3 anions during interactions with circulating pore waters, giving rise to crystalline carbonate-fluorapatite (e.g., Slansky 1986; Froelich et al. 1988; Stalder and Rozendaal 2004). Therefore, low analytical totals may be associated with fine porosity originating during the loss of water from the original gel-like substance.

6. Conclusions

The study represents a contribution to our systematic research of polytypism, chemical composition, and mineralogical association of cronstedtite, with a larger focus on Czech and Slovak localities.

The polytype 1*T* (subfamily C) is the most abundant in the samples studied. The allotwins 1*T*+1*M* (of subfamilies C+A) occur rarely, but they represent the first known examples from the natural terrestrial environment. Previously they were reported from the synthetic run product or meteorite (Müller et al. 1979; Hybler et al. 2018). Disordered allotwins of C+A subfamilies were observed for the first time. The polytype $2H_1$ allotwinned with a small amount of $2H_2$ of the D subfamily is common in many localities but in Litošice occurs rarely. Although the chemical composition of cronstedtite from other localities is usually uniform inside the occurrence, in Litošice, a significant difference was recorded: The subfamily C crystals are relatively rich in Mn (0.2–0.6 *apfu*) and poor in Mg, while the subfamily D crystals are rich in Mg (0.3 *apfu*) and poor in Mn (cf. Tab. 3).

The studied cronstedtite is a part of the symmetrically zoned hydrothermal vein cutting pyrite shales and is associated with abundant Fe–Mn carbonates (rhodochrosite, siderite), opal, quartz, pyrite, and minor magnezite, calcite, and carbonate-fluorapatite. The Fe–Mn carbonates, opal and quartz undoubtedly occur in multiple generations. The textural features, mineral assemblage and chemical composition of vein minerals suggest low temperatures of vein formation. Nevertheless, intense metasomatic replacement of younger portions of cronstedtite filled by opal and siderite was widespread in the studied vein. A distinct unified chemical trend (Mn → Fe → Mg) was observed during each episode of crystallization of carbonates.

Acknowledgments. The first author (JH) thanks late Lubor Žák for providing a part of samples of cronstedtite used for this study. Valuable discussions with Slavomil Ďurovič are highly appreciated, too. Comments and suggestions of two anonymous referees allowed us to improve the manuscript. We thank Libuše Jilemnická and Jana Kotková for critically reading the text. JH acknowledges the project 18-10504S of the Czech Science Foundation and CzechNanoLab Research Infrastructure supported by MEYS CR (LM2018110). This work was also financially supported by the Ministry of Culture of the Czech Republic (DKRVO 2019-2023/1.II.c, 00023272) to JS and ZD.

Electronic supplementary material. Supplementary material consisting of electron microprobe data for

cronstedtite, associated carbonate minerals and apatite are available online at the Journal website (http://dx.doi.org/10.3190/ jgeosci.335).

References

Bailey SW (1969) Polytypism of trioctahedral 1 : 1 layer silicates. Clays Clay Miner 17: 355–371

Bailey SW (1988) Polytypism of 1 : 1 layer silicates. In: Bailey SW (ed) Hydrous Phyllosilicates (Exclusive of Micas). Mineral Soc Amer Rev Mineral Geochem 19: pp 9–27

Barber DJ (1981) Matrix phyllosilicates and associated minerals in C2M carbonaceous chondrites. Geochim Cosmochim Acta 45: 945–970

Bartas F (1955) Annual report of the own exploration of the Semtěš–Sovolusky deposit in 1954. Research report GF P006701, Geofond, Prague (in Czech)

Bartas F (1960) Exploration of pyrite ores Sovolusky. Situation to 1. 1. 1958. Research report GF FZ003885. Geofond, Prague (in Czech)

Bernard JH (1991) Empirical types of ore mineralizations in the Bohemian Massif. Geological Survey, Prague

Bernard JH, Čech F, Dávidová Š, Dudek A, Fediuk F, Hovorka D, Kettner R, Koděra M, Kopecký L, Němec D, Paděra K, Petránek J, Sekanina J, Staněk J, Šímová M (1981) Mineralogy of the Czechoslovakia. Academia, Praha, p 417–418, 441–443

Browning LB, McSween HY Jr, Zolensky ME (1996) Correlated alteration effects in CM carbonaceous chondrites. Geochim Cosmochim Acta 60: 2621–2633

Burbine TH, Burns RG (1994) Questions concerning the oxidation of the ferrous iron in carbonaceous chondrites. In: Abstracts of the 25th Lunar and Planetary Science Conference, held in Houston, TX, 14–18 March 1994, pp 199–200

Calvin WM (1998) Could Mars be dark and altered? Geophys Res Lett 25: 1597–1600

Damour MA (1860) Analyse de la cronstedtite, espèce minérale. Ann Chim Phys 58: 99–103 (in French)

Dornberger-Schiff K, Ďurovič S (1975a) OD-interpretation of kaolinite-type structure – I: symmetry of kaolinite packets and their stacking possibilities. Clays Clay Miner 23: 219–229

Dornberger-Schiff K, Ďurovič S (1975b) OD-interpretation of kaolinite-type structures – II: the regular polytypes (MDO-polytypes) and their derivation. Clays Clay Miner 23: 231–246

Ďurovič S (1981) OD-Charakter, Polytypie und Identifikation von Schichtsilikaten. Fortschr Mineral 59: 191–226 (in German)

Ďurovič S (1997) Cronstedtite-1*M* and coexistence of 1*M* and 3*T* polytypes. Ceramics-Silikáty 41: 98–104

Ďurovič S (2004) Layer stacking in general polytypic structures. In: Prince E (ed) International Tables for Crystallography, Vol. C, Section 9.2.2. 3rd ed., Kluwer, Dordrecht, pp 760–773

Dyl KA, Manning CE, Young ED (2010) The implication of the cronstedtite in water-rich planetesimals and asteroids. In: Astrobiology Science Conference 2010, League City, Texas, Abstract #5627

Fiala F (1951) Diabase and weilburgite rocks of the Lower Ordovician at Chyňava. Sbor Nár Musea v Praze ř B Přír Vědy VII B: 1–42

Fiala F, Kouřimský J (1980) Cronstedtite from Chyňava, ČSSR. Sbor Nár Musea v Praze 36 B: 35–42

Fiala F, Svoboda J (1953) Geological-petrological evaluation of the area between Litošice and Sovolusky in Iron mountains with evaluation of pyrite shales stocks of the C1 and C2 categories. Research report GF FZ000374, Geofond, Prague (in Czech)

Fiala F, Svoboda J (1956) Final report about the exploration of pyrite deposits in the neighbourhood of Litošice in the Iron Mts. Research report GF FZ001449, Geofond, Prague (in Czech)

Froelich PN, Arthur MA, Burnett WC, Deakin M, Hensley V, Jahnke R, Kaul L, Kim K-H, Roe K, Soutar A, Vathakanon C (1988) Early diagenesis of organic matter in Peru continental margin sediments: phosphorite precipitation. Mar Geol 80: 309–343

Geiger CA, Henry DL, Bailey SW, Maj JJ (1983) Crystal structure of cronstedtite-2H_2. Clays Clay Miner 31: 97–108

Gole MJ (1980a) Low-temperature retrograde minerals in metamorphosed Archean banded iron-formations, Western Australia. Canad Mineral 18: 205–214

Gole MJ (1980b) Mineralogy and petrology of very-low metamorphic grade Archean banded iron-formations, Weld Range, Western Australia. Amer Miner 65: 8–25

Hybler J (1998) Polytypism of cronstedtite from Chvaletice and Litošice. Ceramics-Silikáty 42: 130–131

Hybler J (2014) Refinement of cronstedtite-1*M*. Acta Crystallogr B70: 963–972

Hybler J, Sejkora J (2017) Polytypism of cronstedtite from Chyňava, Czech Republic. J Geosci 62: 137–146

Hybler J, Sejkora J, Venclík V (2016) Polytypism of cronstedtite from Pohled, Czech Republic. Eur J Mineral 28: 765–775

Hybler J, Števko M, Sejkora J (2017) Polytypism of cronstedtite from Nižná Slaná, Slovakia. Eur J Mineral 29: 91–99

Hybler J, Klementová M, Jarošová M, Pignatelli I, Mosser-Ruck R, Ďurovič S (2018) Polytypes identification in trioctahedral layer silicates by electron diffraction and application to cronstedtite mineral synthesized by iron-clay interaction. Clays Clay Miner 66: 379–402

Hybler J, Dolníček Z, Sejkora J, Števko M (2020) Polytypism of cronstedtite from Nagybörzsöny, Hungary. Clays Clay Miner 68: 632–645

Hybler J, Dolníček Z, Sejkora J, Števko M (2021) Polytypism of cronstedtite from Ouedi Beht, Morocco. Clays Clay Miner 69:

Janovský JV (1875) Zur Kenntnis des Cronstedtits von Příbram. J Prakt Chem 11: 378–385 (in German)

Kempný J, Grešl J, Odehnal L, Bartas F (1955) Calculation of stocks of pyrite ore in Sovolusky–Semtěš deposit in Iron Mountains. Situation to 1. 1. 1955. Research report GF FZ000852, Geofond, Prague (in Czech)

Lauretta DS, Hua X, Buseck PR (2000) Mineralogy of fine-grained rims in the ALH 81002 CM chondrite. Geochim Cosmochim Acta 64: 3263–3273

López García JA, Manteca JI, Prieto, AC, Calvo B (1992) The first occurrence of cronstedtite in Spain. Structural characterisation. Bol Soc Esp Mineral 15–1: 21–25 (in Spanish)

Mikloš D (1975) Symmetry and Polytypism of Trioctahedral Kaolin-Type Minerals. Unpublished Ph.D. thesis, Institute of Inorganic Chemistry, Slovak Academy of Sciences, Bratislava, pp 1–144 (in Slovak)

Müller WF, Kurat G, Kracher A (1979) Chemical and crystallographical study of cronstedtite in the matrix of the Cochabamba (CM2) carbonaceous chondrite. Tsch Mineral Petrogr Mitt 26: 293–304

Nespolo M, Kogure T, Ferraris G (1999) Allotwinning: oriented crystal association of polytypes – some warnings on consequences. Z Kristallogr 214: 5–8

Novák F, Hoffman, V (1956) Occurence of new minerals in the ore district of the northern part of the Iron Mts. Rozpr Čs Akad Věd, Ř Mat Přír Věd 66: 31–48 (in Czech with an English and Russian abstracts)

Novák F, Jansa J (1965) Paragenesis of minerals with helvine from the Chvaletice deposit. Čas Mineral Geol 10: 75–79 (in Czech)

Novák F, Vtělenský J, Losert J, Kupka F, Valcha Z (1957) Orthochamosite from ore veins in Kaňk near Kutná Hora, a new specific mineral. In: Sborník k osmdesátinám akademika F. Slavíka. Naklatelství ČSAV, Prague, pp 315–343 (in Czech)

Papoušek I (1956a) Deposit of pyrite shales Semtěš–Sovolusky (Sovolusky quarry) in Iron Mts. Research report GF FZ001418, Geofond, Prague (in Czech)

Papoušek I (1956b) Annual report of the own exploration of the Semtěš–Sovolusky deposit in 1955. Research report GF P006063, Geofond, Prague (in Czech)

Papoušek I (1957) Annual report of the geological exploration of the locality Sovolusky–Semtěš in 1956. Research report GF P008551, Geofond, Prague (in Czech)

Pignatelli I, Mugnaioli E, Hybler J, Mosser-Ruck R, Cathelineau M, Michau N (2013) A multi-technique characterisation of cronstedtite synthetized by iron–clay interaction in a step-by-step cooling procedure. Clays Clay Miner 61: 277–289

Pignatelli I, Marrochi Y, Vacher LG, Delon R, Gounelle M (2016) Multiple precursors of secondary mineralogical assemblages in CM chondrites. Meteorit Planet Sci 51–4: 785–805

Pignatelli I, Marrochi Y, Mugnaioli E, Bourdelle F, Gounelle M (2017) Mineralogical, crystallographic, and redox features of the earliest stages of fluid alteration in CM chondrites. Geochim Cosmochim Acta 209: 106–122

Pignatelli I, Mugnaioli E, Marrochi Y (2018) Cronstedtite polytypes in the Paris meteorite. Eur J Mineral 30: 349–354

Pignatelli I, Mosser-Ruck R, Mugnaioli E, Sterpenich J, Gemmi M (2020). The effect of the starting mineralogical mixture on the nature of Fe serpentines obtained during hydrothermal syntheses at 90 °C. Clays Clay Miner 68: 394–412

Pouchou JL, Pichoir F (1985) "PAP" (φρZ) procedure for improved quantitative microanalysis. In: Armstrong JT (ed) Microbeam Analysis. San Francisco Press, San Francisco, pp 104–106

Rigaku Oxford Diffraction (2021) CrysAlisPro version 171.41.93a, Data collection and data reduction GUI

Schulte M, Schock E (2004) Coupled organic synthesis and mineral alteration on the meteorite parent bodies. Meteorit Planet Sci 39: 1577–1590

Slansky M (1986) Geology of sedimentary phosphates. North Oxford Academic, London, pp 1–210

Slavík F (1928) Nerosty z ložisek manganových rud v Železných horách. Čas Nár muz, Odd přírodověd 102: 113–127 (in Czech)

Slavík F (1929) Metallogenese Železných hor. Věda přír X: 9–11 (in Czech)

Stalder M, Rozendaal A (2004) Apatite nodules as an indicator of depositional environment and ore genesis for the Mesoproterozoic Broken Hill-type Gamsberg Zn– Pb deposit, Namaqua Province, South Africa. Miner Depos 39: 189–203

Steinmann JJ (1820) Chemische Untersuchung des Cronstedtit's, eines neuen Fossils von Příbram in Böhmen. Gottlieb Haase, Prague, pp 1–47 (in German)

Steinmann JJ (1821) Chemische Untersuchung des Cronstedtit's, eines neuen Fossils von Pribram in Böhmen. J Chem Phys 32: 69–100 (in German)

Steadman R (1964) The structure of trioctahedral kaolin-type silicates. Acta Crystallogr 17: 924–927

Steadman R, Nuttall PM (1963). Polymorphism in cronstedtite. Acta Crystallogr 16: 1–8

Steadman R, Nuttall PM (1964) Further polymorphism in cronstedtite. Acta Crystallogr 17: 404–406

Varček C, Vasconselos JM, Petrová R, Fejdi P (1990) Cronstedtite $(Fe^{2+}_2Fe^{3+})(SiFe^{3+}O_5)(OH)_4$, from Klement vein, Rožňava. Miner Slov 22: 565–567 (in Slovak)

Vrba K (1886) Vorläufige Notiz über den Cronstedtit von Kuttenberg. Sitz–Ber Kgl Böhm Gessel Wiss 3: 13–19 (in German)

Wahle MW, Bujnowski TJ, Guggenheim S, Kogure T (2010) Guidottiite, the Mn-analogue of cronstedtite: A new serpentine-group mineral from South Africa. Clays Clay Miner 58: 364–376

Weiss Z, Kužvart M (2005) Clay Minerals, Their Nanostructure and Use. Karolinum, Charles University publishing house, Prague, pp 1–281 (in Czech)

Zega TJ, Buseck PR (2003) Fine-grained-rim mineralogy of the Cold Bokkeveld CM chondrite. Geochim Cosmochim Acta 67: 1711–1721

Zolotov MY (2014) Formation of brucite and cronstedtite bearing mineral assemblages on Ceres. Icarus 228: 13–26

Žák L (1955) Alabandite from Litošice, Iron mts. Rozpr Čs Akad Věd, Ř mat přír Věd 66: 49–94 (in Czech with English and Russian abstracts)